# Microlocal analysis of $d$-plane transform on the Euclidean space

HIROYUKI CHIHARA
College of Education
University of the Ryukyus

This is a short summary of our recently published paper [1] (SIAM J. Math. Anal., 2022). We study the basic properties of $d$-plane transform on the Euclidean space as a Fourier integral operator, and its application to the microlocal analysis of streaking artifacts in its filtered back-projection. The $d$-plane transform is defined by integrals of functions on the $n$-dimensional Euclidean space over all the $d$-dimensional planes, where $0 < d < n$. Our results are related to the metal streaking artifacts of CT images, and some generalization of recent results of Park-Choi-Seo [15] (Comm. Pure Appl. Math., 2017) and Palacios-Uhlmann-Wang [14] (SIAM J. Math. Anal., 2018) for the X-ray transform on the plane.

**Acknowledgment**. This work was supported by the Research Institute for Mathematical Sciences, an International Joint Usage/Research Center located in Kyoto University.

# 1 X-ray transform on the plane, CT scanners, and artifacts

This note is based on the basic theory of microlocal analysis. See Hörmander's four volumes of textbooks [9], [10], [11], [12], and the textbooks [2] and [5] on Fourier integral operators.

## 1.1 CT scanners and X-ray transform

We consider two-dimensional CT scanners for cross-sections, and explain that the X-ray transform is considered to be the measurement of CT scanners. In this subsection we assume that the X-ray beam has no width, and traverses the object along a line, say $\gamma$ below. Let $(x, y) \in \mathbb{R}^2$, and let $f(x, y)$ be a compactly supported function describing the attenuation coefficient distribution of the section of an object. We denote by $I_0$ and by $I$ the intensities of the beam before and after passing through the object respectively.

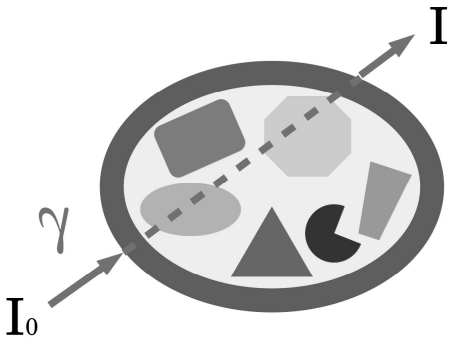


Figure 1. X-ray beam passing though an object

It is well-known that the Beer-Lambert law obtains

$$\log\left(\frac{I_0}{I}\right) = \int_\gamma f. \tag{1}$$

We observe an artificial example of a grayscale image of a cross section, its X-ray transform, the unfiltered back-projection, and the filtered back-projection by using the Julia Programming Language. We introduce the standard coordinates of the space of all the planar lines. For an arbitrary line $\gamma$ in $\mathbb{R}^2$, there exists a pair $(\theta, t) \in [0, 2\pi) \times \mathbb{R}$ such that

$$\begin{aligned}\gamma = L(\theta, t) &= \{(x, y) \in \mathbb{R}^2 \mid x\cos\theta + y\sin\theta = t\} \\ &= \{(x, y) \in \mathbb{R}^2 \mid \cos\theta(x - t\cos\theta) + \sin\theta(y - t\sin\theta) = 0\} \\ &= \{(t\cos\theta - s\sin\theta, t\sin\theta + s\cos\theta) \mid s \in \mathbb{R}\}.\end{aligned}$$

See Figure 2 below. We remark that $L(\theta, t) = L(\theta \pm \pi, -t)$ and $[0, 2\pi) \times \mathbb{R}$ is a double covering of the space of all the planar lines.

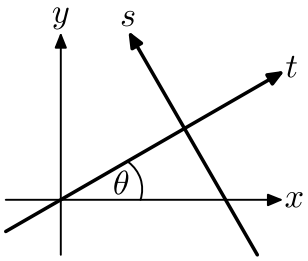


Figure 2. Parametrization $(\theta, t)$ of the space of all the lines in $\mathbb{R}^2$

For an appropriate function $f(x, y)$, the X-ray transform $\mathcal{R}_1 f(\gamma)$ is given by

$$\mathcal{R}_1 f(\gamma) = \mathcal{R}_1 f(\theta, t) := \int_\gamma f = \int_{-\infty}^{\infty} f(t\cos\theta - s\sin\theta, t\sin\theta + s\cos\theta)ds.$$

Then we have $\mathcal{R}_1(\theta, t) = \mathcal{R}_1 f(\theta \pm \pi, -t)$. We have only to consider the coordinates $(\theta, t) \in [0, \pi) \times \mathbb{R}$. The formal adjoint $\mathcal{R}_1^*$ is given by

$$\mathcal{R}_1^* F(x, y) = \frac{1}{4\pi}\int_0^{2\pi} F(\theta, x\cos\theta + y\sin\theta)d\theta = \frac{1}{2\pi}\int_0^{\pi} F(\theta, x\cos\theta + y\sin\theta)d\theta$$

for a function $F(\theta, t)$ with $F(\theta, t) = F(\theta \pm \pi, -t)$. It is well-known that we have the inversion formula

$$f(x, y) = (-\partial_x^2 - \partial_y^2)^{1/2}\mathcal{R}_1^*\mathcal{R}_1 f(x, y) = \mathcal{R}_1^*(-\partial_t^2)^{1/2}\mathcal{R}_1 f(x, y).$$

The adjoint $\mathcal{R}_1^*$ and $(-\partial_x^2 - \partial_y^2)^{1/2}\mathcal{R}_1^* = \mathcal{R}_1^*(-\partial_t^2)^{1/2}$ are said to be the unfiltered back-projection and the filtered back-projection respectively. Here is an artificial example of the set of four grayscale images.

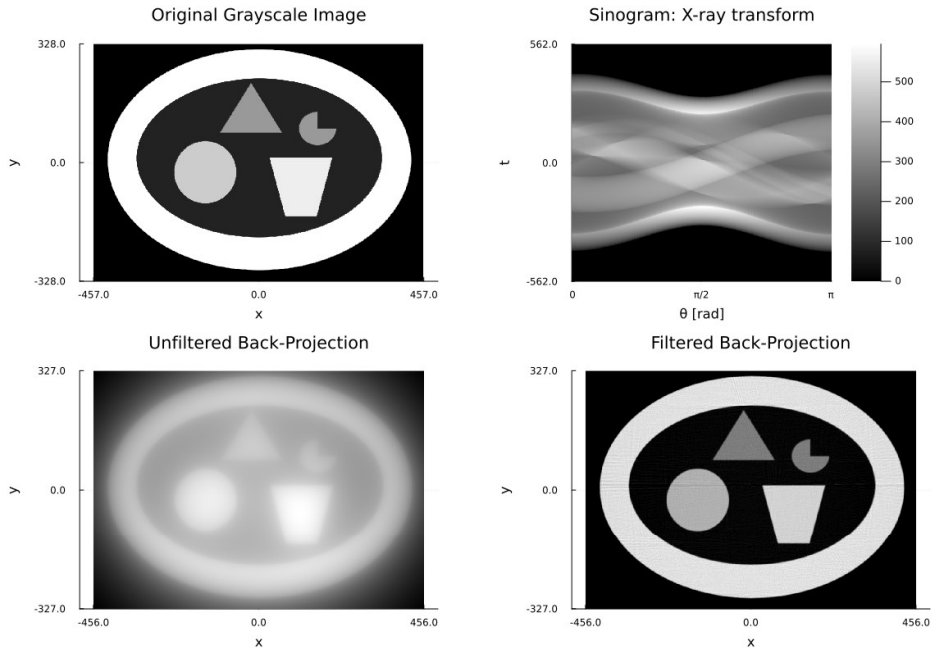


Figure 3. An original gray scale image, its X-ray transform, the unfiltered back-projection, and the filtered back-projection

Here we explain how to see these images.

- **Northwest** A grayscale image is a matrix whose entries are real numbers belonging to the closed interval $[0, 1]$. An element with value $0$ expresses a black pixel, an element with value $1$ expresses a white pixel, and an element with intermediate value between $0$ and $1$ expresses an pixel with corresponding gray color.

- **Northeast** This is the heat map of $\mathcal{R}_1 f(\theta, t)$, that is, the value of each entry of the "matrix" $\mathcal{R}_1 f$ is expressed by the sequential color scale indicated in the color bar. The heat map of X-ray transform is called a sinogram.

- **Southwest** This is the unfiltered back-projection $\mathcal{R}_1^* \mathcal{R}_1 f$. More precisely, this is the grayscale image given by a matrix with modified entries defined by

$$\frac{\mathcal{R}_1^* \mathcal{R}_1 f - \min \mathcal{R}_1^* \mathcal{R}_1 f}{\max \mathcal{R}_1^* \mathcal{R}_1 f - \min \mathcal{R}_1^* \mathcal{R}_1 f},$$

  whose entries are in the interval $[0, 1]$. The grayscale image of $\mathcal{R}_1^* \mathcal{R}_1 f$ is blurred.

- **Southeast** This is the filtered back-projection $(-\partial_x^2 - \partial_y^2)^{1/2} \mathcal{R}_1^* \mathcal{R}_1 f$. Roughly speaking, the first derivative of the unfiltered back-projection is clear and gives the reconstruction of $f$ from the measurement $\mathcal{R}_1 f$. The relationship between unfiltered and filtered back-projections is similar to that of the rectified linear unit (ReLU) and the Heaviside function on $\mathbb{R}$. If we set

$$\mathrm{ReLU}(s) = \begin{cases} s & (s > 0), \\ 0 & (s < 0), \end{cases} \qquad Y(s) = \begin{cases} 1 & (s > 0), \\ 0 & (s < 0), \end{cases}$$

then we have

$$\frac{d}{ds}\mathrm{ReLU} = Y$$

in the sense of distributions. The Heaviside function $Y(s)$ describes the step difference at $s = 0$ clearly, and the ReLU does not.

## 1.2 Metal streaking artifacts

There are some factors causing artifacts in CT images: beam width, partial volume effect, beam hardening, noise in measurements, numerical errors, and etc. See, e.g., Epstein's celebrated textbook on medical imaging [3]. In this note we study the beam hardening effect causing metal streaking artifacts. It is known that this phenomenon occurs for the CT images of human bodies containing metal regions such as implants, stents, metal bones and etc.

In the formulation of (1), the X-ray is supposed to be monochromatic with a fixed energy, say $E_0 > 0$. Actually, however, the X-ray beam has a wide range of energy $E \in [0, \infty)$, and the attenuation coefficient distribution $f_E$ depends on $E$. This is described by the spectral function $\rho(E)$ which is a probability density function of $E \in [0, \infty)$. In this case the formulation of the measurements $P$ of CT scanners becomes

$$P := \log\left(\frac{I_0}{I}\right) = -\log\left\{\int_0^\infty \rho(E)\exp(-\mathcal{R}_1 f_E)dE\right\}.$$

If $f_E$ is independent of $E$, i.e., $f_E = f_{E_0}$, then

$$\begin{aligned}\log\left(\frac{I_0}{I}\right) &= -\log\left\{\int_0^\infty \rho(E)dE \cdot \exp(-\mathcal{R}_1 f_{E_0})\right\} \\ &= -\log\big\{\exp(-\mathcal{R}_1 f_{E_0})\big\} = \mathcal{R}_1 f_{E_0}.\end{aligned}$$

Recently, the beam hardening effect and metal streaking artifacts were studied from the viewpoint of microlocal analysis. Let $D$ be a metal region in $\mathbb{R}^2$. Consider a simple model of spectral function and beam hardening effect of the form

$$\begin{aligned}\rho(E) &= \frac{1}{2\varepsilon}\chi_{[E_0-\varepsilon, E_0+\varepsilon]}(E), \\ f_E(x) &= f_{E_0}(x) + \alpha(E - E_0)\chi_D(x),\end{aligned}$$

where $f_{E_0}$ is an attenuation coefficient distribution of normal human tissue, $\varepsilon$ and $\alpha$ are small positive constants, and $D$ is a metal region which is a disjoint union of finitely many strictly convex bounded domains with smooth boundaries. Then the measurement $P$ becomes

$$P - \mathcal{R}_1 f_{E_0} = -\log\left\{\frac{\sinh(\alpha\varepsilon\mathcal{R}_1\chi_D)}{\alpha\varepsilon\mathcal{R}_1\chi_D}\right\} = \sum_{k=1}^{\infty} A_k(\alpha\varepsilon\mathcal{R}_1\chi_D)^{2k}.$$

This means that $P$ consists of the normal tissue part and the beam hardening part, and that the latter part is a (formal) power series of $\big(\mathcal{R}_1\chi_D\big)^2$. The main object is the filtered back-projection of the power series. Here are pioneering works on the microlocal analysis of metal streaking artifacts for this simple model.

- Park, Choi, and Seo ( [15] Comm. Pure Appl. Math., 2017) proved that the metal streaking artifacts are propagation of $\mathrm{WF}(\chi_D)$ along the union of the common tangential lines $\mathcal{L}$ of metal domains.
- Palacios, Uhlmann, and Wang ( [14] SIAM J. Math. Anal., 2018) proved that the streaking artifacts are conormal distributions supported by $\mathcal{L}$.

The following figure illustrates a grayscale image of two disks of metal regions with different radii, its X-ray transform, the filtered back-projection, and the filtered back projection of $\left(\mathcal{R}_1\chi_D\right)^2$, which is the principal part of the beam hardening effect. The southeast image illustrates the streaking artifacts of four common tangential lines of the two disks.

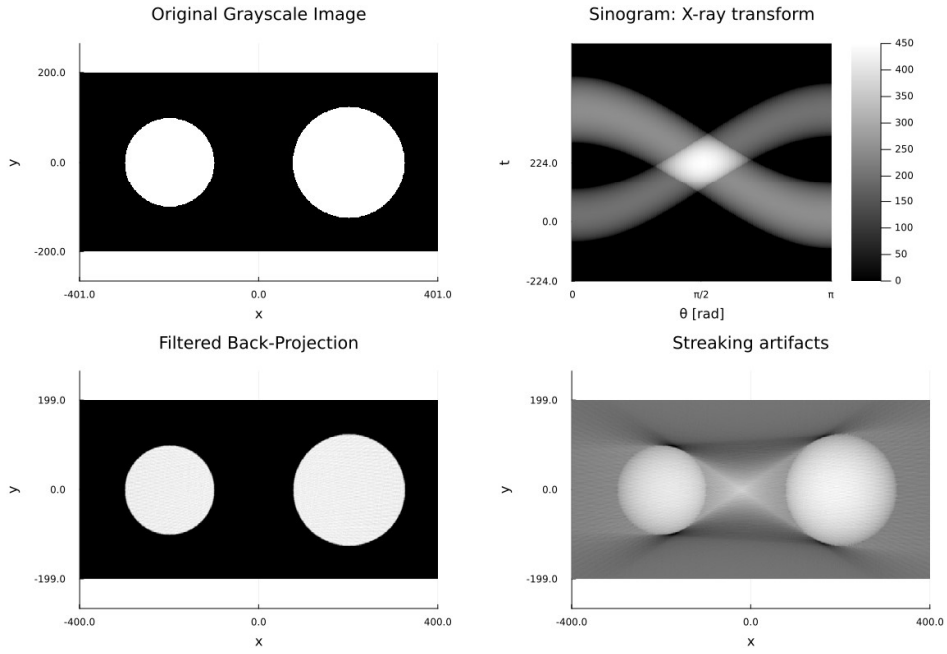


Figure 4. Two disks, the sinogram, the standard FBP, and the FBP of $\left(\mathcal{R}_1\chi_D\right)^2$.

In this note we study the higher dimensional generalization of [14].

## 2 $d$-plane transform

In this section we introduce the $d$-plane transform on the $n$-dimensional Euclidean space, and review the basic facts about CT scanners. Let $n = 2, 3, 4, \ldots$, and let $d = 1, \ldots, n-1$. We denote by $G_{d,n}$ the Grassmannian which is the set of all $d$-dimensional vector subspaces of $\mathbb{R}^n$. It is well-known that $\dim G_{d,n} = d(n-d)$. The affine Grassmannian is the set of all $d$-dimensional planes in $\mathbb{R}^n$, that is,

$$G(d,n) = \{x'' + \sigma \ : \ \sigma \in G_{d,n}, x'' \in \sigma^\perp\},$$

where $\sigma^\perp$ is the orthogonal complement of $\sigma$ in $\mathbb{R}^n$. Set

$$N(d,n) := \dim G(d,n) = (d+1)(n-d)$$

for short. We use notation $x''+\sigma=(\sigma,x'')$.

We fix arbitrary $\sigma\in G_{d,n}$, and divide $x\in\mathbb{R}^n$ as $x=x'+x''\in\sigma\oplus\sigma^\perp=\mathbb{R}^n$. The $d$-plane transform of a function $f(x)=f(x'+x'')=\mathcal{O}(\langle x\rangle^{-d-\varepsilon})$ is defined by

$$\mathcal{R}_d f(\sigma,x'):=\int_{x''+\sigma} f=\int_\sigma f(x'+x'')dx', \tag{2}$$

where $\langle x\rangle=\sqrt{1+|x|^2}$ and $dx'$ is the Lebesgue measure on $\sigma$. In particular $\mathcal{R}_1 f$ is called the **X-ray transform** of $f$, and $\mathcal{R}_{n-1}f$ is called the **Radon transform** of $f$.

Next we explain the inversion formula of $\mathcal{R}_d$. Roughly speaking, the formal adjoint of $\mathcal{R}_d$ is given as integrals of functions over the set of all $d$-planes passing through arbitrary fixed point $x\in\mathbb{R}^n$. More precisely

$$\begin{aligned}\mathcal{R}_d^*\varphi(x)&:=\frac{1}{C(d,n)}\int_{\{\Xi\in G(d,n):x\in\Xi\}}\varphi(\Xi)d\mu(\Xi)\\&=\frac{1}{C(d,n)}\int_{O(n)}\varphi(x+k\cdot\sigma)dk,\end{aligned}$$

where $\varphi\in C\big(G(d,n)\big)$, $C\big(G(d,n)\big)$ is the set of all continuous functions on $G(d,n)$, $C(d,n)=(4\pi)^{d/2}\Gamma(n/2)/\Gamma\big((n-1)/2\big)$, $\Gamma(\cdot)$ is the gamma function, $O(n)$ is the orthogonal group, $d\mu$ and $dk$ are the normalized measures which are invariant under rotations, and $\sigma\in G_{d,n}$ is arbitrary. The inversion formula of $\mathcal{R}_d$ is given as follows.

**Proposition 1** ( [8, Theorem 6.2]). *For $f(x)=\mathcal{O}(\langle x\rangle^{-d-\varepsilon})$*

$$f=(-\Delta_x)^{d/2}\mathcal{R}_d^*\mathcal{R}_d f=\mathcal{R}_d^*(-\Delta_{x''})^{d/2}\mathcal{R}_d f,$$

*where $-\Delta_x=-\partial_{x_1}^2-\cdots-\partial_{x_n}^2$ and $-\Delta_{x''}$ is the Laplacian on $\sigma^\perp$.*

Operators $\mathcal{R}_d^*$ and $(-\Delta_x)^{d/2}\mathcal{R}_d^*=\mathcal{R}_d^*(-\Delta_{x''})^{d/2}$ are said to be the unfiltered back-projection operator and the filtered back-projection operator respectively.

# 3 Conormal distributions

Comparing unfiltered and filtered back projections, one can understand that singularities are the essential part of information contained in imaging data. In this note we quantitatively deal with generalized functions or the distribution kernels of linear operators. So we use the classifications of Schwartz distributions based on singular supports, singular directions, and the order of singularities. These are called the classes of Lagrangian distributions. This section provides preliminaries. we mainly pick up conormal distributions, which are simple examples of Lagrangian distributions.

**Definition 2** (Conormal distributions)**.** Let $X$ be an $N$-dim manifold, and let $Y$ be a closed submanifold of $X$. A Schwartz distribution $u\in\mathscr{D}'(X)$ is said to be conormal with respect to $Y$ of degree $m$ if

$$L_1\cdots L_M u\in{}^\infty H^{\mathrm{loc}}_{(-m-N/4)}(X)$$

for all $M=0,1,2,\dots$ and all vector fields $L_1,\dots,L_M$ tangential to $Y$. Denote by $I^m(X;N^*Y)$, the set of all distributions on $X$ conormal with respect to $Y$ of degree $m$.

Note that $N_y^*Y := T_y^*X/T_y^*Y$ for any $y \in Y$, and

$$\|u\|_{\infty H_{(s)}(\mathbb{R}^N)} := \sup_{j=0,1,2,\dots} \left( \int_{A_j} \langle \xi \rangle^{2s} |\hat{u}(\xi)|^2 d\xi \right)^{1/2},$$

$$A_0 := \{|\xi| < 1\}, \quad A_j := \{2^{j-1} \leqq |\xi| < 2^j\}, j = 1, 2, 3, \dots .$$

Roughly speaking, a conormal distribution $u \in I^m(X; N^*Y)$ is a distribution on $X$ such that $u \in C^\infty(X \backslash Y)$, that is, $\operatorname{singsupp} u \subset Y$, and the microlocal singularities of $u$ on $Y$ are limited to the normal directions of $Y$. If $u \in I^m(X; N^*Y)$, then $\mathrm{WF}(u) \subset N^*Y \setminus 0$. It is very interesting that conormal distributions can be characterized by oscillatory integrals locally.

**Proposition 3** ( [11, Theorem 18.2.8]). *Let $x = (x', x'') \in \mathbb{R}^k \times \mathbb{R}^{N-k}$ and let $Y = \{0\} \times \mathbb{R}^{N-k} = \{x' = 0\}$. Then $u \in \mathscr{D}'(\mathbb{R}^N)$ belongs to $I^{m+k/2-N/4}(\mathbb{R}^N; N^*Y)$ if and only if there exists an amplitude $a(x'', \xi') \in S^m(\mathbb{R}^{N-k} \times \mathbb{R}^k)$ such that*

$$u(x) = \int_{\mathbb{R}^k} e^{ix' \cdot \xi'} a(x'', \xi') d\xi'.$$

Here $S^m(\mathbb{R}^{N-k} \times \mathbb{R}^k)$ is the standard symbol class, that is, we say that a smooth function $a(x'', \xi')$ belongs to $S^m(\mathbb{R}^{N-k} \times \mathbb{R}^k)$ if for any compact set $K \subset \mathbb{R}^{N-k}$ and for any multi-indices $\alpha'$ and $\beta''$, there exists a constant $C(K, \alpha, \beta) > 0$ such that

$$|\partial_{x''}^{\beta''} \partial_{\xi'}^{\alpha'} a(x'', \xi')| \leqq C(K, \alpha, \beta) \langle \xi' \rangle^{m - |\alpha'|}, \quad (x'', \xi') \in K \times \mathbb{R}^k.$$

We can replace the conormal bundle $N^*Y$ by more general conic Lagrangian submanifold $\Lambda$. The elements of $I^m(X; \Lambda)$ is said to be Lagrangian distributions on $X$. These are characterized as oscillatory integrals with more general phase functions of the form:

$$u(x) = \int e^{i\phi(x,\theta)} a(x, \theta) d\theta.$$

The distribution kernels of Fourier integral operators are Lagrangian distributions.

We now see typical examples of conormal distributions.

**Example 4** (A characteristic funtion of a smooth domain). *If $D$ be a domain in $\mathbb{R}^n$ with smooth boundary, then the characteristic function $\chi_D$ of $D$ belongs to $I^{-1/2-n/4}\big(\mathbb{R}^n; N^*\partial D\big)$.*

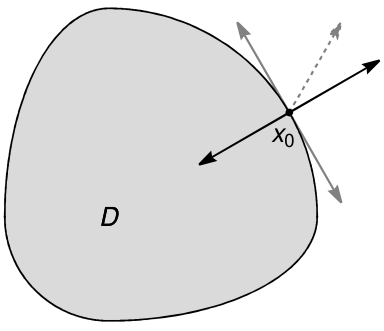


*Figure 5. A bounded domain with smooth boundary, and smooth and singular directions*

**Example 5** (The distribution kernal of a pseudodifferential operator)**.** *Set*

$$\Delta = \{(x, x) : x \in \mathbb{R}^N\},$$

*which is the diagonal part of* $\mathbb{R}^N \times \mathbb{R}^N$*. If* $a(x, \xi) \in S^m(\mathbb{R}^N \times \mathbb{R}^N)$*, then*

$$K(x, y) = \int_{\mathbb{R}^N} e^{i(x-y)\cdot\xi} a(x, \xi) d\xi \in I^m(\mathbb{R}^N \times \mathbb{R}^N; N^*\Delta),$$

$$N^*\Delta = \{(x, x; \xi, -\xi) : x, \xi \in \mathbb{R}^N\}.$$

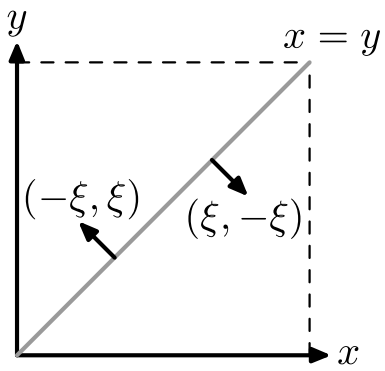


*Figure 6. The singular support of the distribution kernel of a pseudodifferential operator*

# 4 Main Theorem

In this section we state our main theorem of this note, and explain its meaning using some figures. Firstly we state our assumption about the metal region, and set some notation.

**Assumption**. The metal region $D \subset \mathbb{R}^n$ is supposed to be a disjoint union of finitely many $D_j$ $(j = 1, \ldots, J)$ which are simply connected, strictly convex, and bounded with smooth boundaries $\Sigma_j := \partial D_j$. Set $\Sigma := \partial D$.

Denote by $\nu(y_j)$ the unit outer normal vector of $\Sigma_j$ at $y_j \in \Sigma_j$. We consider the set of pairs $(y_j, y_k) \in \Sigma_j \times \Sigma_k$ such as

$$\mathcal{M}_{jk}^{(\pm)} := \{(y_j, y_k) \in \Sigma_j \times \Sigma_k \ : \ y_j + T_{y_j}\Sigma_j = y_k + T_{y_k}\Sigma_k,\ \nu(y_j) = \pm\nu(y_k)\}.$$

We can confirm that this is an $(n-2)$-dimensional submanifold of $\Sigma_j \times \Sigma_k$. Using this we can introduce the set of lines

$$\mathcal{L}_{jk}^{(\pm)} := \{y_j + t(y_k - y_j) \ : \ (y_j, y_k) \in \mathcal{M}_{jk}^{(\pm)},\ t \in \mathbb{R}\},$$

Then $\mathcal{L}_{jk}^{(\pm)}$ becomes a cylindrical surface or a cone which is tangent to $\Sigma_j$ at $y_j$ and to $\Sigma_k$ at $y_k$ for all $(y_j, y_k) \in \mathcal{M}_{jk}^{(\pm)}$. Set $\mathcal{L}_{jk} := \mathcal{L}_{jk}^{(+)} \cup \mathcal{L}_{jk}^{(-)}$ and $\mathcal{L} := \bigcup_{j<k} \mathcal{L}_{jk}$.

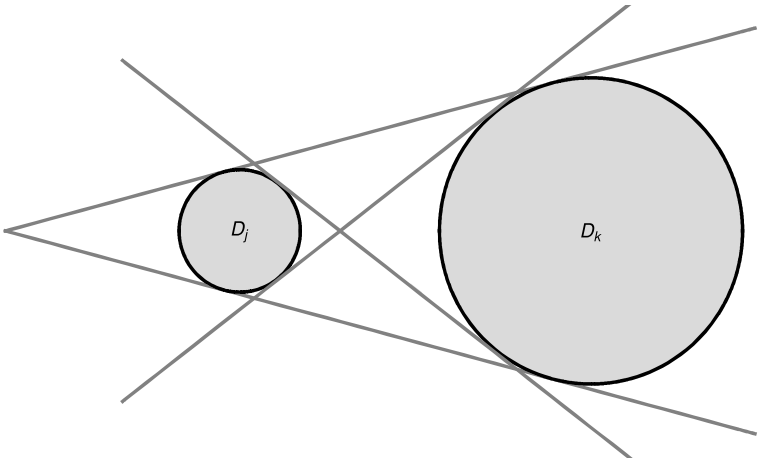


Figure 7. $\Sigma_j$, $\Sigma_k$, $\mathcal{L}^{(+)}_{jk}$, and $\mathcal{L}^{(-)}_{jk}$

We set the notation for the CT image corresponding to the beam hardening effect as a formal series of the form

$$f_{MA} := f_{CT} - f_{E_0} = \sum_{k=1}^{\infty} A_k (a\varepsilon)^{2k} \mathcal{R}_d^* (-\Delta_{x''})^{d/2} [(\mathcal{R}_d \chi_D)^{2k}],$$

where $A_k$ ($k = 1, 2, 3, \dots$), $a$, and $\varepsilon$ are real-valued constants. We now state our main theorem.

**Theorem 6.** *Away from* $\Sigma$*,*

$$f_{MA} \in I^{-(d+2+n/4)+d(n-d)/2}(\mathbb{R}^n; N^* \mathscr{L}).$$

*The principal symbol of the FBP of* $(\mathcal{R}_d \chi_D)^2$ *does not vanish.*

All the known results related to our main theorem are limited to the case $(n, d) = (2, 1)$.

- Park, Choi, and Seo ( [15], 2017) proved that $\mathrm{WF}(f_{\mathrm{MA}}) \subset N^* \mathscr{L}$.
- Palacios, Uhlmann, and Wang ( [14], 2018) proved Theorem 6.
- Wang and Zou ( [16], 2021) studied the studied the case that $D_1, \dots, D_J$ are not necessarily convex. This is difficult setting, and they obtained some results.

We explain what Theorem 6 says.

- **Type A**. If $\Sigma_j$ and $\Sigma_k$ have a common tangential hyperplane, then the common conormal singularity propagates all over the line connecting the tangential points. This is the true identity of the metal streaking artifacts.

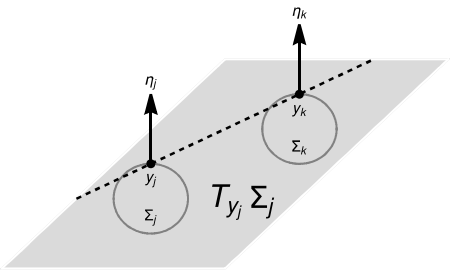


Figure 8. The case that there exists a common hyperplane passing through $y_j$ and $y_k$ for $(y_j, y_k) \in \mathcal{M}^{(\pm)}_{jk}$, that is, $\nu(y_j) = \nu(y_k)$ or $\nu(y_j) = -\nu(y_k)$.

- **Type B**. If $\Sigma_j$ and $\Sigma_k$ have a common tangential plane of codimension two, then the normal directions at the tangential points are different and no singularity propagates along the connecting line.

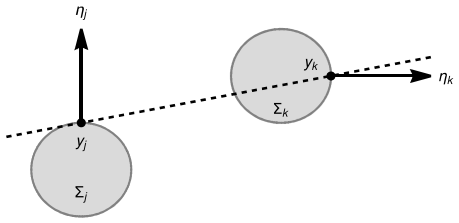


Figure 9. The case that there is not a common hyperplane passing through $y_j$ and $y_k$ for $(y_j, y_k) \in \mathcal{M}_{jk}^{(\pm)}$, that is, $\nu(y_j) \neq \nu(y_k)$ and $\nu(y_j) \neq -\nu(y_k)$.

Finally we state the keys of the proof of Theorem 6.

**Outline of the Proof of Theorem 6.** The main part of the beam hardening effect $f_{MA}$ is the FBP of the power series of $(\mathcal{R}_d\chi_D)^2$. So we check the microlocal singularities arising from the interaction of nonlinearities, and compute the composition of the canonical relation of $\mathcal{R}_d^*$ and the microlocal singularities of the interactions. Roughly speaking the interaction of $(\mathcal{R}_d\chi_D)^2$ is the existence of common tangential lines of Type A or Type B. The canonical relation of $\mathcal{R}_d^*$ accepts all the Type A interactions, and rejects all the Type B interactions. This is the outline of the proof of Theorem 6. For this purpose we need to do the following.

- We could not find the concrete expression of the canonical relation of the $d$-plane transform except for $d = n-1$. So we introduce our original local coordinates of $T^*\big(G(d,n)\big)$, which are convenient to deal with the canonical relation of $\mathcal{R}_d$ in $T^*\big(\mathbb{R}^n \times G(d,n)\big) \setminus 0$, and we compute the canonical relation concretely.

- We investigate the microlocal interactions using paired Lagrangian distributions, which was developed in Melrose and Uhlmann [13], and Greenleaf and Uhlmann [4].

The latter one is basically the same as the planar case [14]. □

# References


[1] H. Chihara, *Microlocal analysis of $d$-plane transform on the Euclidean space*, SIAM J. Math. Anal., **54** (2022), pp.6254–6287.

[2] J. J. Duistermaat, "Fourier Integral Operators", Birkhäuser, Boston, 1995.

[3] C. L. Epstein, "Introduction to the Mathematics of Medical Imaging, Second Edition", SIAM, Philadelphia, 2008.

[4] A. Greenleaf and G. Uhlmann, *Recovering singularities of a potential from singularities of scattering data*, Comm. Math. Phys., **157** (1993), pp.549–572.

[5] A. Grigis and J. Sjöstrand, "Microlocal Analysis for Differential Operators: An Introduction", Cambridge University Press, Cambridge, 1994.

[6] V. Guillemin and S. Sternberg, "Geometric Asymptotics", Mathematical Surveys, **14**, American Mathematical Society, Providence, RI, 1977.

[7] V. Guillemin and G. Uhlmann, *Oscillatory integrals with singular symbols*, Duke Math. J., **48** (1981), pp.251–267.

[8] S. Helgason, "Integral Geometry and Radon Transforms", Springer-Verlag, New York, NY, 2011.

[9] L. Hörmander, "The Analysis of Linear Partial Differential Operators I", Springer-Verlag, Berlin, 1983.

[10] L. Hörmander, "The Analysis of Linear Partial Differential Operators II", Springer-Verlag, Berlin, 1983.

[11] L. Hörmander, "The Analysis of Linear Partial Differential Operators III", Springer-Verlag, Berlin, 1985.

[12] L. Hörmander, "The Analysis of Linear Partial Differential Operators IV", Springer-Verlag, Berlin, 1985.

[13] R. Melrose and G. Uhlmann, *Lagrangian intersection and the Cauchy problem*, Comm. Pure Appl. Math., **32** (1979), pp.483–519.

[14] B. Palacios, G. Uhlmann and Y. Wang, *Quantitative analysis of metal artifacts in X-ray tomography*, SIAM J. Math. Anal., **50** (2018), pp.4914–4936.

[15] H. S. Park, J. K. Choi and J. K. Seo, *Characterization of metal artifacts in X-ray computed tomography*, Comm. Pure Appl. Math., **70** (2017), pp.2191–2217.

[16] Y. Wang and Y. Zou, *Streak artifacts from nonconvex metal objects in X-ray tomography*, Pure Appl. Anal., **3** (2021), pp.295–318.

HIROYUKI CHIHARA
Colloge of Education
University of the Ryukyus
Nishihara, 903-0213 Okinawa, Japan